Ionizing radiation-dependent and independent phosphorylation of the 32 kDa subunit of replication protein A during mitosis.

Holger Stephan[1], Claire Concannon[1], Elisabeth Kremmer[2], Michael P. Carty[3], and Heinz-Peter Nasheuer[1*]

[1]Cell Cycle Control Laboratory, School of Natural Sciences, National University of Ireland, Galway, Galway, Ireland, [2]Helmholtz Zentrum München-Deutsches Forschungszentrum für Gesundheit und Umwelt (GmbH), Marchioninistr. 25, 81377 München, Germany, [3]DNA Damage Response Laboratory, School of Natural Sciences, National University of Ireland, Galway, Galway, Ireland,

[*]To whom correspondence should be addressed: Dr. Heinz-Peter Nasheuer; Cell Cycle Control Laboratory, School of Natural Sciences, National University of Ireland, Galway, Galway, Ireland. Tel: +353-91-49-2430; Fax: +353-91-49-5504; Email: h.nasheuer@nuigalway.ie

ABSTRACT

The human single-stranded DNA binding protein, replication protein A (RPA), is regulated by the N-terminal phosphorylation of its 32kDa subunit, RPA2. RPA2 is hyperphosphorylated in response to various DNA-damaging agents and also phosphorylated in a cell cycle-dependent manner during S- and M-phase, primarily at two CDK consensus sites, S23 and S29. Here we generated two monoclonal phospho-specific antibodies directed against these CDK sites. These phosphospecific RPA2-(P)-S23 and RPA2-(P)-S29 antibodies recognized mitotically phosphorylated RPA2 with high specificity. In addition, the RPA2-(P)-S23 antibody recognized the S-phase-specific phosphorylation of RPA2, suggesting that during S-phase only S23 is phosphorylated, whereas during M-phase both CDK sites, S23 and S29, are phosphorylated. Immunofluorescence microscopy revealed that the mitotic phosphorylation of RPA2 starts at the onset of mitosis, and dephosphorylation occurs during late cytokinesis. In mitotic cells treated with ionizing radiation (IR), we observed a rapid hyperphosphorylation of RPA2 in addition to its mitotic phosphorylation at S23 and S29, associated with a significant change in the subcellular localization of RPA. Our data also indicate that the RPA2 hyperphosphorylation in response to IR is facilitated by the activity of both ATM and DNA-PK, and is associated with activation of the Chk2 pathway.

INTRODUCTION

DNA in cells is challenged by various environmental and cellular stresses causing DNA lesions. Therefore, mechanisms to maintain genome stability are important for cell viability and survival. DNA damage induces numerous cellular responses and leads to cell cycle arrest, DNA repair or the induction of programmed cell death (1). In mammalian cells, the phosphatidylinositol 3-kinase-like kinases (PIKKs) including DNA-dependent protein kinase (DNA-PK), Ataxia-telangiectasia-mutated protein (ATM), and Ataxia-telangiectasia and Rad3-related protein (ATR) play important roles in the DNA damage checkpoint regulation following DNA damage. They phosphorylate several key proteins involved in the DNA damage response such as the tumour suppressor protein p53, checkpoint kinases Chk1 and Chk2, histone H2AX and replication protein A (RPA) (1-4).

RPA, the human single-stranded DNA (ssDNA) binding protein, is a stable heterotrimer consisting of three subunits with apparent molecular masses of 70, 32 and 14kDa (RPA1, RPA2 and RPA3, respectively) (5). RPA is one of the key players in various processes of DNA metabolism including the initiation and elongation of DNA replication, homologous recombination (HR), nucleotide excision repair (NER) and long-patch base excision repair (BER) (6-8). Studies in yeast and mammalian systems indicate that RPA is also involved in DNA damage recognition and checkpoint activation (9-11). The RPA-ssDNA complex generated in response to DNA lesions is implicated in localization of ATR–ATRIP to sites of DNA damage and Rad9-Hus1-Rad1 together with TopBP1 to sites of DNA damage for the activation of ATR (10,12-15). In the following, the RPA2 subunit undergoes hyperphosphorylation in response to DNA-damaging agents, such as UV- and γ-irradiation, DNA-alkylating agents and replication stress (4,16-18). Various members of the PIKK family such as DNA-PK, ATM and ATR have been found to phosphorylate the N-terminal residues of RPA2 *in vitro* and putatively *in vivo* (19-21). A number of different possible phosphorylation sites in the N-terminus of RPA2 were identified using mass spectrometry analysis and two-dimensional phosphopeptide mapping, which revealed four phosphorylation sites (S4, S8, T21 and S33) and a fifth site at either S11, S12 or S13 (18,19,22). It has been demonstrated *in vivo* that an RPA2 mutant that mimics the hyperphosphorylation at the N-terminus of RPA2 is unable to localize to the replication centers in cells, but is capable of association with DNA damage foci (23,24). This is consistent with the

finding that RPA2 hyperphosphorylation after DNA damage disrupts RPA interaction with DNA polymerase α *in vitro* (25). Previous reports suggested that in response to DNA damage, hyperphosphorylation of RPA2 disrupts its association with replication centres during S-phase and contributes to the inhibition of DNA replication (23,24).

RPA2 is also phosphorylated in a cell cycle-dependent manner during S- and M-phase primarily at two CDK consensus sites, S23 and S29, by Cdk1-cyclin B or Cdk2-cyclin A (26-29). Replacement of the CDK consensus sites S23 and S29 by alanine abolishes RPA2 phosphorylation during S-phase (17,28). Although RPA is phosphorylated during initiation of DNA replication (30), N-terminal deletion (residues 2 to 30), or alanine substitutions at S23 and S29 of RPA2 had no significant effect on the ability of RPA to bind ssDNA or to support SV40 DNA replication *in vitro* (31,32). In contrast, recent findings suggested that phosphorylated RPA has a significantly decreased ability to bind and destabilize duplex DNA compared to the unphosphorylated form of RPA (22,29). Additional data showed further that interactions of the N termini of RPA1 and RPA2 are probably important to prevent interference of the phoshorylated RPA2 with the functions of the core DNA-binding domain of RPA (33). Moreover, RPA purified from mitotic cells showed a reduced binding to ATM, DNA polymerase α, and DNA-PK as compared to unphosphorylated recombinant RPA (29).

Although the response of RPA to various DNA damaging agents has been investigated for more than a decade, our knowledge relates to cells in interphase and far less is known about the DNA damage response of RPA in mitosis. To investigate the role of RPA2 phosphorylation in response to DNA damage in mitosis, we have established two novel monoclonal phosphospecific antibodies, RPA2-(P)-S23 and RPA2-(P)-S29, and examined the localization of RPA throughout mitosis. Here, we demonstrate that when DNA damage occurs in mitosis, mitotically phosphorylated RPA2 is additionally hyperphosphorylated and re-localizes to damaged chromosomal DNA. In addition, our results show that ATM and DNA-PK are required for RPA2 hyperphosphorylation in mitosis and that this is associated with an activation of the Chk2-pathway. Based on these observations, we propose that hyperphosphorylation of RPA2 may play a role in DNA repair during mitosis.

MATERIALS AND METHODS

Cell Culture and cell lines – Cells were maintained at 37°C in a humidified atmosphere containing 5% CO_2. Human HeLa S3 cells were grown in Dulbecco's minimal essential medium (DMEM; Lonza Ltd). EBV-transformed lymphoblastoid cells from A-T (GM O1525) and Seckel syndrome (GM 18367) patients and control cells (GMO7521), abbreviated as LC, were obtained from ATCC and cultured in RPMI-1640 medium (Lonza Ltd). DMEM and RPMI-1640 medium were supplemented with 10% fetal bovine serum (FBS; Lonza Ltd) and antibiotics Penicillin/Streptomycin (Sigma-Aldrich; 100 IU/ml and 100 mg/ml, respectively).

Expression vectors and transfection – The full-length ATR cDNA (pcDNA3-ATR) vector and the full-length ATM cDNA expression vector (pMEP4) under the control of heavy metal-inducible metallothionein promoter were kind gifts from Drs. P. A. Jeggo and M. F. Lavin, respectively, and were described previously (34-37). ATM-deficient cells stably expressing full-length ATM were generated as described previously (37). To obtain Seckel cells stably expressing full-length ATR, 2×10^6 exponentially growing Seckel cells were transfected using FuGene-HD (Roche) with 6 µg of pcDNA3-ATR DNA according to the manufacturer's instructions. Then cells were cultivated over 3-4 weeks in media containing G-418 (Sigma-Aldrich; 600 µg/ml) starting 48 h after transfection and monitored by immunoblot. Stable clones were maintained in RPMI-1640 medium supplemented with G-418 (400 µg/ml).

Synchronization of cells – To obtain mitotically arrested cells, exponentially growing HeLa S3 cells were treated with nocodazole (100 ng/ml final concentration; Sigma-Aldrich) for 16 h (38). Mitotic cells were separated from interphase cells by shaking the semi-detached mitotic cells off the dish ("shake-off") and collected by centrifugation at 160×*g* for 5 min. To release mitotic cells from nocodazole block, cells were washed once with pre-warmed phosphate-buffered saline (PBS) for 2 min and twice with pre-warmed serum-free medium for 2 min and then plated into serum-containing medium. To obtain a cell population enriched in S-phase, HeLa S3 cells were synchronized by a double thymidine-block as previously described by (39). To achieve highly enriched mitotic populations of lymphoblastoid cells including stably transfected cell lines two consecutive cell cycle blocks were performed. A thymidine treatment for 19 h with 2

mM thymidine was followed by a release for 3 hr in thymidine-free medium. Then the cells were incubated with nocodazole (100 ng/ml) for 12 h.

Cell treatment – Cells were treated with 10 Gray (Gy) of ionizing radiation (IR) (dose rate of 2.75 Gy/min) in the presence of serum-containing medium, using a ^{137}Cesium source (Mainance Engineering Ltd., UK) at room temperature. PIKK inhibitor wortmannin (Sigma-Aldrich), ATM-inhibitor KU-55933 and DNA-PK-inhibitor NU7441 (both provided by KuDOS Pharmaceuticals Ltd, Cambridge) were dissolved as stock solution of 10mg/ml in DMSO. Where indicated, mitotically arrested HeLa S3 cells were pretreated, 1 h prior to IR, with wortmannin, KU-55933, NU7441 or with DMSO as solvent control to analyze RPA2 phosphorylation. NU7441 was derived from NU7026 and has been shown to be a potent radiosensitiser by specifically inhibiting DNA-PK (40-42) while KU-55933 is a specific and very potent small molecule inhibitor of ATM (40,43). Roscovitine (Calbiochem), a CDK inhibitor (44), solubilized in DMSO was used in the indicated concentrations.

Flow cytometry – Cells were harvested by trypsination or mitotic shake off, washed in ice-cold PBS, and fixed in 70% ethanol at -20°C. The fixed cells were then collected by centrifugation at 300×*g* for 5 min, washed once in PBS and resuspended in 1ml propidium iodide/RNase staining solution (BD Pharmingen) followed by incubation for 30 minutes at room temperature in darkness. The cell cycle stage was determined by flow cytometry using a FACS Calibur (BD Pharmingen). Data were analyzed using Cell Quest™ Software (BD Pharmingen).

Purification of RPA and Cdk1-cyclin B kinase - Recombinant human RPA heterotrimer was expressed and purified from *Escherichia coli* BL21 (DE3) cells transformed with p11d-tRPA vector (kindly provided by Dr. Marc Wold) as described previously (45,46). Cdk1-cyclin B kinase was expressed in insect cells and purified as described previously (47).

***In vitro* kinase assays** - The *in vitro* kinase reactions were carried out as previously described (48,49) using 100 ng of purified RPA as a substrate and 2 µg purified Cdk1-cyclin B.

Kinase assays with immunoprecipitated kinase were carried out as described (38). The Cdk1 were immunoprecipitated with protein G plus/protein A-agarose (Calbiochem) using 1000 µg of total protein in 1 ml of HeLa S3 cell extracts, 4 µg of anti-Cdk1 antibody ([C-19], Santa Cruz Biotechnology, Inc.) and 1 µg purified recombinant histone H1 (kindly provided by Dr. Andrew Flaus) per reaction.

Antibody generation - To analyze the mitotic phosphorylation of RPA2, rat monoclonal phosphospecific anti-RPA2-(P)-S23 [clone RBP-8H3] and anti-RPA2-(P)-S29 [clone RBP-8C7] antibodies were raised against two synthetic RPA2 phosphopeptides containing phosphor-S23 or phosphor-S29, respectively. The anti-RPA1 [RAC-4D9] antibody was previously described (50,51). In addition, rat monoclonal anti-RPA2 [clone RBF-4E4] and anti-RPA3 [clone RCF-7H5] antibodies were raised against the respective recombinant full-length proteins. Hybridoma cell lines producing monoclonal antibodies were established according to standard procedures (52).

Immunoblotting - Cells were washed once in ice-cold PBS and lysed in lysis buffer (PBS containing 1% Triton X-100, 0.5% sodium deoxycholate (DOC), 0.1% sodium dodecyl sulphate (SDS)) supplemented with 10 mM NaF, 1 mM Na_3VO_4, 10 mM β-glycerophosphate, 1× Phosphatase Inhibitor Cocktail I and 1× Protease Inhibitor Cocktail (both Sigma-Aldrich). Whole cell lysates were then clarified by centrifugation at 14,000×*g* for 10 min at 4°C. Equal amounts of cell lysates (20 µg) were separated on 12% SDS-polyacrylamide gels (29:1 acrylamide/bisacrylamide), transferred to PVDF membranes, and analyzed by antibodies as described earlier (53). As indicated membranes were probed with anti-RPA2 (1/4000 [9H8], Neomarkers), phosphospecific anti-RPA2-(P)-S4/8 (1/4000, Bethyl Laboratories), phosphospecific anti-Chk1-(P)-S317 (1/1500, Cell Signaling Technology, Inc.), anti-Chk1 (1/1500, Cell Signaling Technology, Inc.), phosphospecific anti-Chk2-(P)-T68 (1/1500, Cell Signaling Technology, Inc.), anti-Chk2 (1/1500 [2CHK01], Neomarkers), phosphospecific anti-H3-(P)-S10 (1/2500, Sigma-Aldrich), anti-ATR (1/2000 [N-19], Santa-Cruz biotechnology, Inc.), anti-Cdk1 (1/1500 [C-19], Santa Cruz Biotechnology, Inc.), anti-ATM (1/1000 [ab2631], Abcam), phosphospecific anti-ATM-(S)-1981 (1/1000 [10H11.E12], Abcam), anti-BubR1 (1/1000 [8G1], Abcam), phosphospecific anti-BubR1-(S)-676, (1/1000, kindly provided by Drs. S. Elowe and E. Nigg (54)), or anti-

GAPDH (1/5000 [mAbcam 9484], Abcam) overnight at 4°C. Western blots were then probed with horseradish peroxidase-conjugated secondary antibodies (HRP, Jackson Immuno Research) and visualized using the ECL or ECL Plus chemoluminescent solution (GE Healthcare).

Subcellular fractionation – The subcellular fractionation protocol was adapted from (55). Briefly, 1×10^7 mitotically arrested HeLa S3 cells were washed with PBS, collected at 160×*g*, and resuspended in 1 ml of pre-chilled hypotonic buffer (20 mM Hepes [pH 7.5], 10 mM KCl, 1 mM $MgCl_2$, 0.5 mM EDTA supplemented with 1 mM dithiothreitol (DTT), 10 mM NaF, 1 mM Na_3VO_4, 10 mM β-glycerophosphate, 1× Phosphatase Inhibitor Cocktail I and 1× Protease Inhibitor Cocktail), and incubated on ice for 10 min. All procedures were carried out at 4 °C. Cells were then Dounce-homogenized (with loose fitting pestle) gently by 15-20 strokes. The homogenate was centrifuged at 2,000×*g* for 10 min. The supernatant was then carefully removed, clarified by centrifugation at 14,000 × *g* for 10 min and referred to as "soluble fraction". The pellet of the first centrifugation was then resuspended in 1 ml of hypotonic buffer supplemented with 0.025% Triton-X100 and the tube was rotated for 5 min at 4°C at low speed. Samples were subsequently centrifuged at 2,000×*g* for 5 min at 4°C and the supernatant referred to as "wash fraction". The wash step was repeated once again, but after centrifugation this supernatant was discarded. Finally, the remaining pellet was resuspended in 1 ml homogenization buffer (20 mM Hepes [pH 7.5], 1% SDS 150 mM NaCl, 1 mM $MgCl_2$, 0.5 mM EDTA supplemented with 1 mM DTT, 10 mM NaF, 1 mM Na_3VO_4, 10 mM β-glycerophosphate, 1× Phosphatase Inhibitor Cocktail I and 1× Protease Inhibitor Cocktail) and completely solubilized by brief sonication (10 sec with 50% amplitude; Digital Sonifier® S-250D, Branson,UK) on ice. This sample was referred to as the "chromosomal-bound fraction ".

Immunofluorescence microscopy - Mitotic cells were allowed to attached on poly-L-lysine-coated glass slides and then washed in PBS and fixed with 4% para-formaldehyde in PBS for 15 min at room temperature. After permeabilization with 0.2% Triton X-100 in PBS for 10 min at room temperature, non-specific binding sites were blocked with 10% goat serum (Sigma-Aldrich)/5% BSA (Pierce) in PBS-Tween 20 (0.02%) solution for 30 min at 37°C. Primary antibodies (monoclonal rat anti-RPA2

[RBF-4E4], anti-RPA2-Ser23 [RBP-8H3], anti-RPA2-Ser29 [RBP-8C7]~~),~~ and monoclonal mouse anti-α-tubulin (1/2000 [B-5-1-2], Sigma-Aldrich)) were incubated in 0.05% PBS-Tween 20 overnight at 4 °C. The following day, the cells were washed and stained for 1 h at room temperature with Cy2-conjugated anti-mouse or Cy3-conjugated anti-rat secondary antibodies (1/500, Jackson ImmunoResearch). DNA was counterstained with ToPro3 (1/500, Molecular Probes) in mounting buffer (20 mM Tris-HCl [pH 8.0], 90% glycerol, 200 µM 1,4-diazabicyclo[2.2.2]octane (DABCO)). Confocal 12-bit images (single stacks in Z-dimension, stack size 512×512 pixel) were captured using a Zeiss LSM 510 confocal laser scanning microscope system equipped with a Zeiss Axiovert 200 microscope with a Plan-Apochromat 63×/1.4 oil objective and analyzed with LSM 5 Image Browser software (Carl Zeiss GmbH; Jena, Germany)

RESULTS

Phosphorylation of RPA2 in mitosis

In human and yeast cells it has been reported that RPA2 is phosphorylated in a cell cycle-dependent manner during S- and M-phase. In human cells, two CDK consensus sites, S23 and S29, were phosphorylated in cell cycle-dependent manner (26,28,29). To examine phosphorylation of RPA2 in mitosis, monoclonal phosphospecific antibodies recognizing either RPA2 phosphorylation at Ser23 or Ser29 were produced. Their specificity was verified by immunoblot analysis of asynchronous (*AS*), mitotically (*M*) and S-phase (*S*) arrested cells and purified recombinant human RPA2 (*R*) (Fig. 1A) and by Cdk1-cyclin B *in vitro* kinase assay (Fig. 1B). The quality of cell extracts was assessed using indicated cell cycle markers. As shown in both figures (Fig. 1A and 1B), phosphospecific RPA2-(P)-S23 [RBP-8H3] and RPA2-(P)-S29 [RBP-8C7] antibodies recognized a band corresponding to mitotically phosphorylated RPA2 (marked as *mp*). In addition, very little reactivity of RPA2-(P)-S23 and RPA2-(P)-S29 was observed in asynchronous control cells (Fig. 1A, *lane: AS*) whereas none was detected with purified recombinant human RPA2 (*R*), which represented the basal (no mobility shift) isoform of RPA2 (marked as *b* in Fig. 1A, *lane: R*). In addition, RPA2-(P)-S23 antibody, but not RPA2-(P)-S29, recognized an RPA2 isoform marked as *sp* (Fig. 1A (*lane: AS* and *S*) and Fig. 1B). This isoform is characterized by a small reduction in RPA2 mobility and is mostly present in S-phase-arrested cells (27-29,56) suggesting that only a single CDK site is phosphorylated during S-phase. To exclude cross reactivity of both phospho-specific RPA2 antibodies and their recognition sites (phosphorylated S23 and S29), an *in vitro* kinase assay was performed using Cdk1-cyclin B and three different RPA2 CDK phosphorylation site mutants. As shown in supplementary Fig. S1, no cross reactivity with the unphosphorylated RPA2 or between the phosphorylated sites was detected.

Analysis of *in vitro* CDK-phosphorylated recombinant RPA2 and S-phase phosphorylated RPA2 (Fig. 1B) revealed that anti-RPA2-(P)-S23 antibody detected both phosphorylated forms marked as *sp* to a similar extent as anti-RPA2 antibody. However, it is important to note that the S-phase-phosphorylated RPA2 (*sp*) comprises only about 10 % of the total RPA2 in the analyzed S-phase-enriched cell population (Fig. 1B). Altogether, these findings let us suggest that during S-phase only S23 is phosphorylated whereas during M-phase both CDK sites, S23 and S29, are phosphorylated.

Since both newly generated phosphospecific RPA2 antibodies were successfully employed in immunoblot, they were also used to investigate the localization of mitotically phosphorylated RPA2 throughout different stages of M-phase by immunofluorescence microscopy. It has been previously reported that mitotic phosphorylation appears at the G2- to M-phase transition (29), but how mitotically phosphorylated RPA is distributed in comparison to heterotrimeric RPA, and, moreover, when the dephosphorylation of RPA2 takes place are still under discussion. As shown in Fig. 1C, RPA2 was excluded from the mitotic chromosomes throughout mitosis (for comparison see α-tubulin staining in supplementary Fig. S2). The two other subunits of RPA, RPA1 and RPA3, were also excluded from the chromosomes (see supplementary Fig. S3A). In addition, using both phosphospecific RPA2 antibodies, a sharp decrease of mitotically phosphorylated RPA2 was observed at the end of cytokinesis when chromosomal DNA de-condenses (Fig. 1C). Moreover, these data reveal that in early G1-phase RPA2 is dephosphorylated and re-enters the newly reformed nucleus (Fig. 1C). These findings indicate that all three events: dephosphorylation of mitotic RPA2, de-condensation of mitotic chromosomes and re-localization of RPA occur simultaneously. However, the correlation between the RPA2 dephosphorylation and the de-condensation of mitotic chromosomes needs to be examined further.

Mitotic RPA is hyperphosphorylated and changes its localization in response to DNA damage

The role of RPA in DNA replication and DNA damage response during interphase has been investigated for more than a decade (9,11). However, far less is known about the response of RPA when the DNA damage occurs in mitosis. To investigate the response of RPA after DNA damage in mitosis, asynchronous or mitotically arrested HeLa S3 cells were either mock- or IR-treated. As shown in Fig. 2, treatment of asynchronous and mitotic cells with IR leads to RPA2 hyperphosphorylation, detected as a slower migrating RPA2 isoform (marked as form *hp*) and with an anti-RPA2-(P)-S4/8 antibody. Interestingly, both newly generated anti-RPA2-(P)-S23 and anti-RPA2-(P)-S29 antibodies recognized RPA2 hyperphosphorylation only in mitotic cells exposed to IR. These findings indicate that, in addition to its mitotic phosphorylation at S23 and S29, RPA2 ~~is~~ becomes hyperphosphorylated when DNA damage is induced in mitosis. Since earlier reports showed alterations of RPA localization in response to DNA

damage during interphase, we wanted to determine whether RPA re-localization takes place in mitosis. Therefore, we carried out immunofluorescence microscopy analysis of mitotic cells subjected to γ-irradiation. In unirradiated mitotic cells, RPA2 was excluded from prometaphase chromosomes, as determined by staining with anti-RPA2-(P)-S23, anti-RPA2-(P)-S29 and anti-RPA2 antibodies (Fig. 3A, *panels: mock-treated*). In contrast, in cells exposed to IR, mitotically phosphorylated RPA2 changes its distribution and co-localizes with chromosomes (Fig. 3A, *panels: IR-treated*), which was observed within 20 min post-irradiation (data not shown). These results suggest that RPA containing mitotically phosphorylated RPA2 does not associate with chromatin and chromosomal DNA in unirradiated mitotic cells (Figure 3B, and 3A) but binds to chromatin (Figure 3B, lane 8) and localizes with chromosomes (Figure 3A, 4th column of panels) after IR.

To provide additional evidence for these findings, we performed subcellular fractionations of mitotic cells that were either mock-treated or exposed to IR. The purity of the soluble and chromatin-bound protein fractions was verified by immunoblot using anti-GAPDH and anti-H3-(P)-S10 antibodies, respectively. Chromatin-bound proteins were solubilized by sonication (Fig. 3B), or alternatively by DNase I treatment (supplementary Fig. S3B). In the case of mock-treated cells, mitotically phosphorylated RPA2 was present mainly in the soluble fraction and with much lower intensity in the wash fraction (Figs. 3B and S3B). In addition, trace amounts of "basal" RPA2 was detected in the chromosomal fraction. In contrast to unirradiated cells, the distribution of RPA2 between the different fractions was altered after IR treatment, with hyperphosphorylated RPA2 being detected predominantly in the chromatin-bound fraction. In the remaining insoluble fraction after DNAse I treatment, no RPA subunit was detected either in mock- or IR-treated cells (Fig. S3B). These observations further support our findings that RPA binds to chromosomal DNA in mitotic cells in response to IR whereas in unirradiated mitotic cells RPA does not. In addition, we found that the RPA1 and RPA3 subunits were redistributed in a pattern similar to RPA2 (Figs. 3B, S3A, and S3B), which suggests that RPA in mitosis is present as a heterotrimeric complex. The localization data on all three RPA subunits contradict previous study (57) but are consistent with the finding that RPA could be biochemically purified as a stable heterotrimeric complex from mitotic cells by others and by us (29,58,59). The results obtained here indicate that DNA damage in mitotic cells leads to an association of RPA

with chromatin. In addition to its mitotic phosphorylation, RPA2 is also hyperphosphorylated after exposure of cells in M-phase to ionizing radiation.

S23 and S29 are not phosphorylated in response to DNA damage caused by IR in asynchronous cells

Recently published results indicate that CDKs and PIKKs are involved in RPA2 phosphorylation in response to genotoxic stress (26). To investigate whether IR-treated asynchronous cells exhibit a similar response, we analyzed RPA2 phosphorylation status in mock- or IR-treated cells in the presence or absence of the CDK inhibitor roscovitine. As shown the Fig. 3C, no RPA2 phosphorylation at S29 was detected in asynchronous cells. The low S23 phosphorylation signal of the *sp* migrating RPA2 form was due to the presence of S-phase cells and was not perturbed by IR or roscovitine treatment. RPA2 hyperphosphorylation and phosphorylation of ATM, Chk2 and H2AX (at S1981, T68 and S139, respectively) were seen only in IR-treated cells (Fig. 3C). Strikingly, hyperphosphorylation of RPA2 and phosphorylation of H2AX, but not ATM and Chk2, exhibited elevated levels with increasing doses of roscovitine after IR treatment. In addition, inhibition of Cdk1 activity by roscovitine was monitored using immunoprecipitated Cdk1 as a kinase source and histone H1 as a substrate (Fig. 3C, bottom). The Cdk1-associated incorporation of [^{32}P] phosphate into histone H1 was strongly reduced when cells were treated with increasing doses of roscovitine. This result is in agreement with previous findings that roscovitine inhibits CDKs and forms a tight complex, which can be immunoprecipitated, and that the CDK inhibition can be measured in a kinase assay in vitro (60,61). In contrast, IR-treatment itself did not display any noticeable effect on the Cdk1 activity in vitro (Fig. 3C). These findings suggest that CDKs are not involved in RPA2 hyperphosphorylations in response of interphase cells to IR, which is in agreement with the knowledge that CDKs are not activated after IR (62).

DNA damage during mitosis leads to delay in mitotic progression and checkpoint activation

To further investigate the response of human RPA to DNA damage in mitosis, mitotically arrested HeLa S3 cells were either mock- or IR-treated with 10 Gy (see supplementary Fig. S4 for cell viability) and then released from nocodazole arrest to allow cells to progress throughout mitosis. In the case of mock-treated cells,

dephosphorylation of mitotically phosphorylated RPA2 was detected 1 h post-release. By 3 h post-nocodazole release the majority of RPA2 was found in the dephosphorylated RPA2 form (*form b*) consistent with the cells having exited mitosis (Fig. 4A,). Mitotic cells exposed to IR showed a delay in dephosphorylation of mitotically phosphorylated RPA2 in comparison to mock-treated cells (Fig. 4A, see supplementary Fig. S5, quantification of the mitotic RPA2 phosphorylated form). IR treatment of mitotic cells resulted in the appearance of RPA2 hyperphosphorylation 1 h post release, which decreased over time and was not detected after 4 h post release (Fig. 4A). Interestingly, a similar pattern of dephosphorylation was observed for the mitotically phosphorylated RPA2, suggesting that both phosphorylation signals are abolished when cells exit mitosis. The latter is in agreement with immunofluorescence microscopy analyses performed with these antibodies (Supplementary Fig. S2) showing the phosphorylation of RPA2 at sites S23 and S29. The phosphorylation of histone H3 at position S10 also declined with similar kinetics, as determined by western blotting (Fig. 4A). To monitor the activation of the spindle assembly checkpoint in mock- and IR-treated mitotic cells, anti-BubR1 and anti-BubR1-(P)-S676 antibodies were used. Cells exposed to IR showed extended checkpoint activation with BubR1 phosphorylation detected up to 4 h post nocodazole release whereas in mock-treated cells BubR1 phosphorylation was abolished 2 h post-release (Fig 4A).

To support the hypothesis that the prolonged mitotic RPA2 phosphorylation was associated with a delay in mitotic progression caused by DNA damage, we also monitored cell cycle progression by flow cytometry (Fig. 4B). FACS analysis revealed that by 3 h post-nocodazole release the majority of unirradiated cells exited mitosis, with only ~33% of cells remaining in mitosis (Fig. 4B and 4C). In contrast, cells subjected to IR were delayed in mitotic exit, e.g. at 3 h post-release ~52% of cells still remained in mitosis (Fig. 4B and 4C). These results revealed that DNA damage generated by IR leads to delay in mitotic progression. The differences between the numbers of cells in G_2/M and in G_1 in the mock- and IR-treated cell populations were statistically significant (Student's t test, $p \leq 0.01$ for all time points t > 0h).

Since we observed that hyperphosphorylation of RPA2 in response to DNA damage occurs within the first hour (Fig. 4A), we examined RPA2 hyperphosphorylation in nocodazole-released cells every 15 min during the first hour after IR treatment. In addition, cells kept in nocodazole block were subjected to a similar treatment to

investigate the effect of sustained mitotic arrest on the RPA2 hyperphosphorylation response. As shown in Fig. 5A, RPA2 hyperphosphorylation occurred already in the first 15 min post-irradiation in both arrested and released cells, which indicates a rapid DNA damage response.

To directly compare the DNA damaging effect of IR and bleomycin, mitotically arrested HeLa cells were exposed to both DSBs agents and than released from the nocodazole block. Immunoblot analyses revealed that the extent of RPA2 hyper-phosphorylation was very similar after IR- and bleomycin treatments (Fig. 4D). However, the mitotic and S4/S8 phosphorylation were abolished after 4h in case of IR-treated mitotic cells, indicating that cells entered G1-phase, whereas RPA2 from bleomycin-treated cells still showed a significant mitotic and S4/S8 phosphorylation at a time point of 8 h post treatment and nocodazole release of the cells (Fig. 4D).

In mammalian cells, DNA damage results in the activation of DNA damage check-points, which are regulated by checkpoint kinases ATM and ATR, and subsequently phosphorylate the two signal-transducing kinases Chk1 and Chk2 (1). We assessed the activation of the DNA damage checkpoint in mitosis by analyzing phosphorylation of Chk1 and Chk2 with phosphospecific S317 and T68 antibodies, respectively (Fig. 5B). Interestingly, prometaphase-arrested cells showed only very low levels of Chk1 activation in response to IR, whereas cells released from the mitotic block displayed rapid phosphorylation of the kinase. In contrast, Chk2 phosphorylation following IR treatment was observed at similar levels in both mitotically arrested cells and cells released from nocodazole arrest. The only difference applied to the 60 min time point when the level of Chk2 phosphorylation was noticeably decreased in cells kept under mitotic arrest in comparison to cells released from nocodazole arrest (Fig. 5B compare left and right panel).

The results obtained here reveal that IR-treated cells released from a mitotic block show Chk1 and Chk2 activation and RPA2 hyperphosphorylation. Since nocodazole-arrested cells exhibit only Chk2 activation and RPA2 hyperphosphorylation, our findings suggest that the RPA2 hyperphosphorylation associated with the Chk2-pathway.

ATM and DNA-PK are involved in hyperphosphorylation of RPA2 in mitosis

ATM and DNA-PK have been implicated in the hyperphosphorylation of RPA2 that follows DNA damage induced during interphase (17,63,64). To elucidate whether these

PIKKs play also a role in the hyperphosphorylation of RPA2 in mitosis, we first investigated the effect of wortmannin, an inhibitor of PIKKs (65), on RPA2 hyperphosphorylation. HeLa S3 cells arrested in mitosis were incubated with different doses of wortmannin or DMSO as solvent control 1 hour prior to γ-irradiation. It has been shown that wortmannin at a dose of 20 μM efficiently inhibits ATM and DNA-PK, whereas ATR is only partially affected at this concentration (65). As shown in Fig. 6A, DNA damage-induced RPA2 hyperphosphorylation was observed within 1 hour post-irradiation in IR-treated cells but was not seen in mock-treated cells. Wortmannin doses of 10 and 20 μM effectively reduced the RPA2 hyperphosphorylation induced by IR to a level below detection but did not have any impact on the mitotic phosphorylation. These findings indicate that ATM, DNA-PK, or both kinases are involved in RPA2 hyperphosphorylation in mitosis after IR treatment.

To further elucidate the role of these kinases, we used the specific inhibitors for ATM and DNA-PK, KU-55933 and NU7441, respectively (see supplementary Fig. S6 for cell viability after drug treatment). Both drugs were applied to cells in a manner similar to wortmannin. The IC_{50} values for inhibition of ATR kinase activity by NU7441 or KU-55933 are greater than 100 μM, and ATR activity should not be inhibited under the present conditions (42,43). As shown in Fig. 6B, inhibition of ATM by KU-55933 and DNA-PK by NU7441 caused a strong reduction of RPA2 hyperphosphorylation but did not affect the mitotic phosphorylation. Similar results were obtained when cells were incubated with caffeine (data not shown). 20 μM of DNA-PK and ATM inhibitors did not completely inhibit hyperphosphorylation of RPA2 in IR-treated cells whereas the same doses of wortmannin reduced the hyperphosphorylation of RPA2 to a level below detection.

To investigate the involvement of the ATR kinase, Seckel, A-T and control (LC) cells were compared for their ability to hyperphosphorylate RPA2 in response to IR in mitotic cells. The expression levels of both PIKKs were monitored using anti-ATM and anti-ATR antibodies. Examination of RPA2 in mitotic cells after exposure to IR revealed an impaired hyphosphorylation in A-T cells whereas Seckel and LC cells showed a robust RPA2 response (Fig. 6C). Introduction of exogenic ATM into A-T cells, fully restores their ability to hyperphosphorylate RPA2 after IR treatment to levels similar to those seen in Seckel and LC cells. Seckel cells stably expressing transgenic ATR showed no significant increase in the RPA2 hyperphosphorylation in response to

IR. Following IR treatment, phosphorylation of ATM at S1981 was observed in Seckel, LC and A-T cells stably transfected with ATM. Our results suggest that the mitotic hyperphosphorylation of RPA2 in response to IR is mediated by ATM and DNA-PK rather than ATR.

DISCUSSION

The role of the cell cycle-dependent phosphorylation of RPA has been in the centre of interest in the fields of DNA replication, DNA repair and DNA damage signaling for more than a decade (9,11). The establishment of phosphospecific antibodies has previously provided a better understanding of DNA damage-dependent RPA phosphorylation. To enhance the knowledge of the cell cycle regulation of RPA, two novel monoclonal RPA2 antibodies were produced against two characterized CDK sites, S23 and S29, RBP-8H3 and RBP-8C7, respectively. Both phosphospecific antibodies recognized mitotically phosphorylated RPA2, confirming that mitotic phosphorylation of RPA2 includes phosphorylation on S23 and S29 (26,28,29). The RPA2-(P)-S23 antibody also detected a characteristic RPA2 isoform present during S-phase, however with lower intensity. This would be consistent with a smaller fraction of RPA2 being phosphorylated in S-phase cells compared to mitotic cells (9). *In vitro* phosphorylation using Cdk1 and various purified RPA2 phosphorylation site mutants indicated that S23 or S29 are phosphorylated by this kinase (Supplementary Fig. S1), which supports the findings of other researchers (17,19), and that both monoclonal antibodies presented here effectively discriminate between the two sites. Our results suggest that S23 is phosphorylated in S- and M-phase, whereas S29 phosphorylation only takes place during M-phase. These findings are in agreement with results of Fang and Newport showing that RPA2 shares phosphorylation sites in S-phase and mitosis (30). They also identified an additional site specifically phosphorylated in mitosis by Cdk1, but did not determine the exact site *in vivo* (30).

Our analysis revealed that both antibodies are very suitable for microscopic analyses. The mitotic phosphorylation of RPA2 lasts throughout mitosis until late stages of M-phase suggesting a specific dephosphorylation mechanism of RPA2 late in mitosis as supported by the analyses of mitotic spindles in parallel (for α-tubulin staining see supplementary Fig. S2). Mitotically phosphorylated RPA is excluded from chromosomes and the nuclear scaffold and is maintained within the soluble cellular fraction. This might be necessary to avoid possible interference of RPA with mitotic processes such as condensation of chromosomes. It has been shown that mitotically phosphorylated RPA binds to dsDNA with lower affinity than non-phosphorylated RPA (29). Late in cytokinesis dephosphorylation of RPA2 takes place, probably during chromosome de-condensation, and RPA2 dephosphorylated at S23 and S29 re-enters

the newly formed nucleus. Our findings and studies of other researchers have shown that the RPA expression levels do not fluctuate during the cell cycle, especially during mitosis (28,29,66). These data lead us to hypothesize that, most likely at the end of cytokinesis, a rapid dephosphorylation of RPA2 takes place, rather than proteolysis and new synthesis of RPA2 and its subunits. Since RPA2 is phosphorylated during the entire M-phase, starting in early mitosis and lasting until all M-phase-associated processes are finalized (Supplementary Fig. S2). We propose that the phosphospecific RPA2-(P)-S23 and RPA2-(P)-S29 antibodies described here should be excellent M-phase markers, which is supported by western blotting of RPA2 and other mitotic marker such as histone H3 phosphorylation (Fig. 4A).

The response of RPA to various DNA-damaging events is well established in interphase cells, but very little is known about its response to DNA damage that occurs during M-phase. Using phosphospecific RPA2 antibodies, we observed, in addition to phosphorylation at S23 and S29, a rapid RPA2 hyperphosphorylation response following IR treatment during mitosis. Moreover, RPA changes its subcellular localization in response to IR, from chromatin-excluded to chromatin-associated. In the case of UV treatment (dose of 5 - 15 J/m^2), no RPA2 hyperphosphorylation and changes of localization were observed in mitotic cells (data not shown). These findings indicate that RPA might be involved in the cellular DNA response and DNA repair processes during mitosis, supporting its role in DSBs repair pathways found in interphase cells. Anantha *et al*. (26) showed that genotoxic stress generated in or before S-phase by camptothecin and bleomycin caused RPA2 hyperphosphorylation and phosphorylation at S29. They suggested that cell cycle-dependent phosphorylation is a requirement for the hyperphosphorylation in response to DNA damage. In contrast, our results did not find an involvement of CDKs in the RPA2 hyperphosphorylation after IR treatment in asynchronous cells. Firstly, the RPA2 hyperphosphorylation mobility shift observed in asynchronous cells exposed to IR did not comprise phosphorylation at S23 and S29. Secondly, the level of RPA2 hyperphosphorylation was elevated in IR- and roscovotine-treated cells further supports our findings. This is consistent with the knowledge that the cellular response to DNA damage after IR includes the degradation of Cdc25A and a lack of activation of CDKs (62). The apparent contradiction may reflect different requirements for DNA damage signaling after the different DNA damaging agents used: IR (this study and those reviewed in (62)), and camptothecin and bleomycin (26). Contrary to interphase cells, after IR treatment of cells in mitosis, the

hyperphosphorylated, shifted form of RPA2 contained phosphorylated S29-most likely since mitotic RPA2 is already modified by CDKs. In agreement with our result, S29 phosphorylation of RPA2 was also observed in bleomycin-treated mitotic cells (67).

DNA damage occurring during mitosis leads to checkpoint activation and a delay in mitotic exit (68-70). We observed an IR-induced delay in dephosphorylation of mitotic RPA when cells pass through M-phase. This was due to a prolonged mitotic progression. However, hyperphosphorylation and CDK-dependent phosphorylation of RPA2 was only observed in mitotic cells exposed to IR. When cells entered the new cell cycle, RPA2 hyperphosphorylation, the mitotic shift of RPA2 and phosphorylation of H3 at position S10 were diminished suggesting that only cells with repaired DSBs might enter G1. Liu and Weaver (17) showed that the earliest RPA2 hyperphosphorylation was detected in interphase cells 45 min post IR treatment with a dose of 50 Gy. In contrast, using lower doses such as 10 Gy, RPA2 hyperphosphorylation was not detected until 2 h and peaked at 3-4 h after IR treatment (17,63). Strikingly, we observed IR-induced hyperphosphorylation of RPA2 already at 15 min post treatment (starting at 5-10 min, data not shown) in both mitotically arrested cells and cells released from mitotic block. These results indicate that mitotic cells are able to induce RPA2 hyperphosphorylation in response to IR treatment more rapidly than interphase cells. Mitosis is a very short and vulnerable cell cycle stage, which may require a very fast DNA damage response by DNA repair proteins including RPA. Interestingly, only IR-treated cells released from the mitotic block showed Chk1 and Chk2 activation, whereas nocodazole-arrested cells exhibited only Chk2 activation. These results suggest that in order to activate an IR-induced DNA damage response and subsequently Chk1, cells might have to progress through mitosis and pass the spindle checkpoint. We could show the activation of the spindle checkpoint in progressing mitotic cells treated with IR by monitoring BubR1 phosphorylation status. In contrast, in response to IR, Chk2 activation might be triggered independently from the Chk1 pathway during mitosis. It has been shown that both downstream checkpoint kinases are differently regulated in response to DNA damage during the cell cycle (71,72). Our data suggest that the DNA damage response of RPA2 is associated with Chk2 activation in mitotic cells. This is in line with a previous report, which proposed that mitotic entry after IR is linked with inactivation and dephosphorylation of Chk1 (73). The results presented here are further supported by findings of Zachos *et al*. (74), who examined the mitotic function of Chk1 using the chicken DT40 system. They proposed a role for

Chk1 in the spindle checkpoint, specifically in delaying anaphase onset by regulation of Aurora-B and BubR1. This would suggest that cells which pass the spindle checkpoint are able to activate Chk1. Using a Chk1 inhibitor in interphase cells (66), the inability of Chk1 activity to modulate IR-induced RPA2 hyperphosphorylation in different cell lines was observed, which is also in line with our findings.

The results presented here reveal that in mitotic cells, hyperphosphorylation of RPA2 in response to IR is mediated through ATM and DNA-PK. In both cases, the inhibition of either ATM or DNA-PK, but not ATR, leads to reduction of RPA2 hyperphosphorylation in M-phase cells after IR treatment. Both members of the PIKK family are also involved in the cellular response to DSBs, and have been shown in interphase cells to phosphorylate RPA2 *in vitro* and/or *in vivo* (17,19,20,63,64). We propose that IR-induced RPA2 hyperphosphorylation in mitosis can be mediated by both ATM and DNA-PK activities.

Taken together, our results indicate the involvement of RPA in a DNA repair process in response to DNA damage occurring in mitosis. It will be interesting in future experiments to assess the precise roles of RPA in response to ionising radiation in mitotic cells, including a putative function in promoting DSB repair during mitosis.

ACKNOWLEDGEMENTS

We wish to thank Drs. A. Stephan, C. Morrison and S. Cruet-Hennequart for the careful reading of this manuscript and helpful discussions. Furthermore, we thank Drs. P. A. Jeggo, M. F. Lavin, K. Weisshart, M. Wold, S. Elowe and E. Nigg for providing reagents and Hemant Kumar (Indian Institute for Technology, Delhi, India) for assistance and practical support. We are grateful to Drs. M. O'Connor and G. Smith (KuDOS Pharmaceuticals Ltd., Cambridge) for generously providing the DNA-PK inhibitor (NU7441) and ATM inhibitor (KU-55933). This work was supported by the Irish Research Council for Science Engineering and Technology (IRCSET), INTAS (Brussels, Belgium), Health Research Board (HRB), Ireland, and Science Foundation Ireland (SFI).

Figure 1. Characterization of phosphospecific antibodies anti-RPA2-(P)-S23 and anti-RPA2-(P)-S29. A. Immunoblots showing the reactivity of phosphospecific anti-RPA2-(P)-S23 and anti-RPA2-(P)-S29 antibodies to RPA2 in asynchronous (*AS*), mitotically (*M*), and S-phase (*S*) arrested cells. In addition, 100 ng of purified human recombinant RPA (*R*) and the reactivities of anti-RPA2 (total, RBF-4E4) antibody served as controls. Detection of phosphospecific H3-(P)-S10, cyclin B1 and cyclin A by the appropriate antibodies were used as cell cycle markers. Detection of GAPDH in different extracts served as a loading control. Abbreviation used in the figure: *hp* – hyperphosphorylated RPA2, *mp* – mitotically phosphorylated RPA2, *sp* – phosphorylated at a single CDK-site of RPA2, *b* – basal RPA2 (no mobility shift). **B**. Reactivity of phosphospecific anti-RPA2-(P)-S23, anti-RPA2-(P)-S29, and total anti-RPA2 antibodies to *in vitro* phosphorylated RPA2 by Cdk1-cyclin B. 100 ng of purified, recombinant RPA2 was phosphorylated by 2 µg purified Cdk1-cyclin B. Then *in vitro* phosphorylated RPA2 and cell extracts obtained from cells arrested in M- and S-phase were analyzed by western blot. The membrane was probed with phosphospecific anti-RPA2-(P)-S29 and horseradish peroxidase coupled secondary antibody and reactivity was detected with ECL. Then the membrane was stripped with Restore Western Blot Stripping Buffer (Pierce) and incubated a second time with anti-RPA2-(P)-S23 antibody to detect RPA2 phosphorylation at S23. After stripping the membrane a second time, it was analyzed with total RPA2 antibody [RBF-E4E] to detect all forms of RPA2. Detection of Cdk1 and cyclin B with specificc antibodies served as controls for active kinase. Phosphorylated RPA2 bands in S-phase cell extracts of the immunoblot were quantified using Image Gauge software (Raytest, Germany) yielding 5 arbitrary units (AU) of RPA2 *sp* form in comparison to 51 AU of *b* form with the anti-RPA2 antibody (total, RBF-4E4). Additionally the antibodies RBF-4E4 and anti-RPA2-(P)-S23 recognized biochemically phosphorylated and *in vivo* phosphorylated RPA2 (*sp* forms) with similar sensitivity (RBF-4E4: 28 AU and 5 AU, anti-RPA2-(P)-S23: 25 AU and 3.5 AU). **C**. Immunolocalization of total and mitotically phosphorylated RPA2 at different stages of M-phase. RPA2 was detected using anti-RPA2-(P)-S23, anti-RPA2-(P)-S29 and total anti-RPA2 [RBF-4E4] primary antibodies and Cy3-labeled secondary antibodies and analyzed by confocal microscopy. DNA was counterstained with ToPro3.

Figure 2. RPA2 is hyperphosphorylated in response to IR in mitosis. Immunoblots showing RPA2 hyperphosphorylation in response to IR as detected by phosphospecific RPA2-(P)-S23 and anti-RPA2-(P)-S29 antibodies. Asynchronous (*AS*) and mitotically arrested (*M*) HeL-S3 cells were mock- or IR-treated (10 Gy) and analyzed 1 h post treatment. Total anti-RPA2 and anti-RPA2-(P)-S4/8 antibodies were employed as control. Recognition of GAPDH served as a loading control. Abbreviations used in the figure: *hp* – hyperphosphorylated RPA2, *mp* – mitotically phosphorylated RPA2, *sp* – RPA2 phosphorylated at a single CDK site, *b* – basal RPA2 (no mobility shift).

Figure 3. RPA2 co-localizes with chromosomal DNA in response to IR in mitotic HeLa S3 cells. A. Images showing changes in the localization pattern of RPA2 in mitotic HeLa S3 cells, which were mock- or IR-treated (10 Gy) and fixed 1 h post-irradiation. RPA2 was detected using an total anti-RPA2 [RBF-4E4], phosphospecific anti-RPA2-(P)-S23 and anti-RPA2-(P)-S29 antibodies. The DNA was counterstained with ToPro-3. **B.** Immunoblot showing subcellular fractionation of mitotic cells mock-treated or exposed to IR (10 Gy). Subcellular localization of RPA subunits was detected using RPA antibodies as indicated. Anti-H3-(P)-S10 and anti-GAPDH antibodies were used as controls. Abbreviations used in the figure: T = whole cell lysates, SF = soluble fraction, WF = wash fraction and CF = chromosomal bound fraction. **C.** RPA2 hyperphosphorylation in response to IR treatment in asynchronous cells. Immunoblot showing RPA2 hyperphosphorylation response of asynchronous HeLa S3 cells in the presence or absence of CDK inhibitor roscovitine after IR treatment. Asynchronous HeLa S3 cells were preincubated for 30 min with 25, 50 and 100 µM of roscovitine or DMSO as solvent control, followed by mock- or IR-treated (10 Gy) and 1 h incubation in the continued presence or absence of roscovitine or in the presence of DMSO as solvent control. Cells were harvested and analyzed by immunoblot using an total RPA2, phosphopecific RPA2-(P)-S4/S8, phosphopecific RPA2-(P)-S23 or phosphopecific RPA2-(P)-S29 antibodies. The activation of the ATM-Chk2 checkpoint pathway was monitored using phosphopecific antibodies ATM-(P)-S1981 and Chk2-(P)-T68. The anti-γH2X antibody was employed as marker for DSBs. Anti-ATM, anti-Chk2 and anti-GAPDH antibody served as loading controls. Abbreviations used in the figure: *AS* – asynchronous cells, *M* – mitotic cells, *D* – DMSO solvent only, *hp* – hyperphosphorylated RPA2, *mp* – mitotically phosphorylated RPA2, *b* – basal RPA2 (no mobility shift). To verify the Cdk1 inhibition by roscovitine, Cdk1 was

immunoprecipitated, and its kinase activity was measured using a histone H1 kinase assays. After SDS-PAGE, the gel was stained with Coomassie blue and incorporation [^{32}P] phosphate into histone H1 was analyzed using a phosphor imager system (Fuji LA 5000, Fuji Europe, Germany) and quantification with ImageGauge software (Fuji Europe, Germany). The Cdk1 activity of the mock-treated sample in absence of roscovitine was arbitrarily defined as 100% Cdk1 activity. The Coomassie blue stain of the gel and the immunoblot with anti-Cdk1 antibody demonstrate that equal amount of H1 and Cdk1, respectively, were present in these reactions (* marks the antibody light chain).

Figure 4. IR treatment of human cells in mitosis leads to delay in mitotic progression and RPA2 hyperphosphorylation. A. Immunoblot showing RPA2 phosphorylation patterns in response to IR treatment in mitosis. Mitotic HeLa S3 cells were obtained by nocodazole arrest for 16 h followed by mitotic shake off. Cells were mock- or IR-treated (10 Gy) and subsequently released from the arrest. Cells were harvested at the indicated time points. Whole cell lysates were analyzed by immunoblot as indicated. The proteins detected by the phosphospecific anti-H3-(P)-S10 antibody and the anti-GAPDH antibody served as mitosis marker and loading control, respectively. **B**. Flow cytometry profiles showing analysis of the cell cycle progression in HeLa S3 cells after release from nocodazole arrest and mock or IR treatment (10 Gy). Representative flow cytometry profile of mock- or IR-treated (10 Gy) HeLa S3 cells over time following nocodazole release. **C**. Diagram showing the quantified average (n=3) of flow cytometry results present in Fig. 4B. Cells in G_2/M-, and G_1-phase are represented as percentage of the total cell population. The differences between the numbers of cells in G_2/M and in G_1 in the mock- and IR-treated cell populations were statistically significant as determined by Student's t test ($p \leq 0.01$ for all time points t > 0h).

Figure 5. IR treatment of cells in mitosis yields a different checkpoint response in nocodazole-arrested and cells released from nocodazole block. Mitotic HeLa S3 cells were mock- or IR-treated (10 Gy) and released from the mitotic arrest or kept in mitotic arrest. Cells were harvested at indicated time points. **A**. Immunoblot showing RPA2 as detected by total anti-RPA2, phosphospecific anti-RPA2-(P)-S4/8, anti-RPA2-

(P)-S23 and anti-RPA2-(P)-S29 antibodies. **B**. Immunoblot showing the checkpoint activation in mitotic cells in response to IR as detected with phosphospecific Chk1-(P)-S317 and Chk2-(P)-T68 antibodies. Antibodies against total Chk1, Chk2 and anti-GAPDH served as loading controls. Abbreviations used in the figure: *hp* – hyper-phosphorylated RPA2, *mp* – mitotically phosphorylated RPA2, *b* – basal RPA2 (no mobility shift).

Figure 6. Involvement of ATM and DNA-PK in hyperphosphorylation of RPA2 after IR treatment of mitotic cells. A. Immunoblot showing RPA2 hyperphos-phorylation response of mitotic HeLa S3 cells in the presence of PIKK inhibitor wortmannin. Mitotically arrested HeLa S3 cells were incubated for 1 h with 5, 10 and 20 μM of wortmannin or DMSO as solvent control prior to mock or IR treatment. At 1 h post-irradiation cells were harvested and analyzed by immunoblot using an total RPA2 or phosphopecific RPA2-(P)-S4/S8 antibodies. Anti-GAPDH antibody served as loading control. **B**. Immunoblot showing the RPA2 hyperphosphorylation response to IR treatment in mitosis in the presence of specific ATM or DNA-PK inhibitors. Mitotically arrested HeLa S3 cells were incubated for 1 h with 5, 10 and 20 μM of ATM-inhibitor (ATMi) KU-55933, DNA-PK-inhibitor (DNA-PKi) NU7441 or DMSO as solvent control alone. Following this treatment, cells were mock- or IR-treated (10 Gy). At 1 h post-irradiation cells were analyzed by immunoblot using a total RPA2 or phosphopecific RPA2-(P)-S4/S8 antibodies. Anti-GAPDH antibody served as loading control. **C.** Immunoblot showing RPA2 hyperphosphorylation response of mitotic Seckel, A-T, and control (LC) cells after IR treatment. Seckel, A-T and LC cells were enriched in mitosis using two consecutive cell cycle arrests (thymidine followed by nocodazole block), followed by mock or IR treatment (10 Gy). Cell extracts were prepared 1 h post-irradiation. RPA2 was analyzed by immunoblot using the indicated antibodies. The expression levels of ATM and ATR were detected with anti-ATM and anti-ATR antibodies. A phosphospecific anti-ATM-(P)-S1981 antibody was employed to monitor DNA damage-dependent phoshorylaiton of ATM. Seckel and A-T cell lines stably transfected with full length ATR (labeled as "+ATR") or ATM (labeled "+ATM") cDNA expression vectors were established, respectively. An anti-GAPDH antibody was used as loading control. Abbreviations used in the figure: *D* – DMSO solvent only, *hp* – hyperphosphorylated RPA2, *mp* – mitotically phosphorylated RPA2, *b* – basal RPA2 (no mobility shift).

REFERENCES

1. Sancar, A., Lindsey-Boltz, L.A., Unsal-Kacmaz, K. and Linn, S. (2004) Molecular mechanisms of mammalian DNA repair and the DNA damage checkpoints. *Annu Rev Biochem*, 73, 39-85.
2. Giaccia, A.J. and Kastan, M.B. (1998) The complexity of p53 modulation: emerging patterns from divergent signals. *Genes Dev*, 12, 2973-2983.
3. Nasheuer, H.P., Smith, R., Bauerschmidt, C., Grosse, F. and Weisshart, K. (2002) Initiation of eukaryotic DNA replication: regulation and mechanisms. *Prog Nucleic Acid Res Mol Biol*, 72, 41-94.
4. Sakasai, R., Shinohe, K., Ichijima, Y., Okita, N., Shibata, A., Asahina, K. and Teraoka, H. (2006) Differential involvement of phosphatidylinositol 3-kinase-related protein kinases in hyperphosphorylation of replication protein A2 in response to replication-mediated DNA double-strand breaks. *Genes Cells*, 11, 237-246.
5. Wold, M.S. (1997) Replication protein A: a heterotrimeric, single-stranded DNA-binding protein required for eukaryotic DNA metabolism. *Annu Rev Biochem*, 66, 61-92.
6. DeMott, M.S., Zigman, S. and Bambara, R.A. (1998) Replication protein A stimulates long patch DNA base excision repair. *J Biol Chem*, 273, 27492.
7. He, Z., Henricksen, L.A., Wold, M.S. and Ingles, C.J. (1995) RPA involvement in the damage-recognition and incision steps of nucleotide excision repair. *Nature*, 374, 566-569.
8. Sigurdsson, S., Trujillo, K., Song, B., Stratton, S. and Sung, P. (2001) Basis for avid homologous DNA strand exchange by human Rad51 and RPA. *J Biol Chem*, 276, 8798-8806.
9. Binz, S.K., Sheehan, A.M. and Wold, M.S. (2004) Replication protein A phosphorylation and the cellular response to DNA damage. *DNA Repair (Amst)*, 3, 1015-1024.
10. Broderick, S., Rehmet, K., Concannon, C. and H.P., N. (2009) In Nasheuer, H. E. (ed.), *Genome Stability & Human Diseases*. Springer, Berlin, Germany, pp. in the press.
11. Fanning, E., Klimovich, V. and Nager, A.R. (2006) A dynamic model for replication protein A (RPA) function in DNA processing pathways. *Nucleic Acids Res*, 34, 4126-4137.
12. Ball, H.L., Myers, J.S. and Cortez, D. (2005) ATRIP binding to replication protein A-single-stranded DNA promotes ATR-ATRIP localization but is dispensable for Chk1 phosphorylation. *Mol Biol Cell*, 16, 2372-2381.
13. Mordes, D.A., Glick, G.G., Zhao, R. and Cortez, D. (2008) TopBP1 activates ATR through ATRIP and a PIKK regulatory domain. *Genes Dev*, 22, 1478-1489.
14. Xu, X., Vaithiyalingam, S., Glick, G.G., Mordes, D.A., Chazin, W.J. and Cortez, D. (2008) The basic cleft of RPA70N binds multiple checkpoint proteins, including RAD9, to regulate ATR signaling. *Mol Cell Biol*, 28, 7345-7353.
15. Zou, L. and Elledge, S.J. (2003) Sensing DNA damage through ATRIP recognition of RPA-ssDNA complexes. *Science*, 300, 1542-1548.
16. Carty, M.P., Zernik-Kobak, M., McGrath, S. and Dixon, K. (1994) UV light-induced DNA synthesis arrest in HeLa cells is associated with changes in phosphorylation of human single-stranded DNA-binding protein. *EMBO J*, 13, 2114-2123.

17. Liu, V.F. and Weaver, D.T. (1993) The ionizing radiation-induced replication protein A phosphorylation response differs between ataxia telangiectasia and normal human cells. *Mol Cell Biol*, 13, 7222-7231.
18. Zernik-Kobak, M., Vasunia, K., Connelly, M., Anderson, C.W. and Dixon, K. (1997) Sites of UV-induced phosphorylation of the p34 subunit of replication protein A from HeLa cells. *J Biol Chem*, 272, 23896-23904.
19. Niu, H., Erdjument-Bromage, H., Pan, Z.Q., Lee, S.H., Tempst, P. and Hurwitz, J. (1997) Mapping of amino acid residues in the p34 subunit of human single-stranded DNA-binding protein phosphorylated by DNA-dependent protein kinase and Cdc2 kinase in vitro. *J Biol Chem*, 272, 12634-12641.
20. Block, W.D., Yu, Y. and Lees-Miller, S.P. (2004) Phosphatidyl inositol 3-kinase-like serine/threonine protein kinases (PIKKs) are required for DNA damage-induced phosphorylation of the 32 kDa subunit of replication protein A at threonine 21. *Nucleic Acids Res*, 32, 997-1005.
21. Unsal-Kacmaz, K. and Sancar, A. (2004) Quaternary structure of ATR and effects of ATRIP and replication protein A on its DNA binding and kinase activities. *Mol Cell Biol*, 24, 1292-1300.
22. Nuss, J.E., Patrick, S.M., Oakley, G.G., Alter, G.M., Robison, J.G., Dixon, K. and Turchi, J.J. (2005) DNA damage induced hyperphosphorylation of replication protein A. 1. Identification of novel sites of phosphorylation in response to DNA damage. *Biochemistry*, 44, 8428-8437.
23. Vassin, V.M., Wold, M.S. and Borowiec, J.A. (2004) Replication protein A (RPA) phosphorylation prevents RPA association with replication centers. *Mol Cell Biol*, 24, 1930-1943.
24. Olson, E., Nievera, C.J., Klimovich, V., Fanning, E. and Wu, X. (2006) RPA2 is a direct downstream target for ATR to regulate the S-phase checkpoint. *J Biol Chem*, 281, 39517-39533.
25. Patrick, S.M., Oakley, G.G., Dixon, K. and Turchi, J.J. (2005) DNA damage induced hyperphosphorylation of replication protein A. 2. Characterization of DNA binding activity, protein interactions, and activity in DNA replication and repair. *Biochemistry*, 44, 8438-8448.
26. Anantha, R.W., Vassin, V.M. and Borowiec, J.A. (2007) Sequential and synergistic modification of human RPA stimulates chromosomal DNA repair. *J Biol Chem*, 282, 35910-35923.
27. Din, S., Brill, S.J., Fairman, M.P. and Stillman, B. (1990) Cell-cycle-regulated phosphorylation of DNA replication factor A from human and yeast cells. *Genes Dev*, 4, 968-977.
28. Dutta, A. and Stillman, B. (1992) cdc2 family kinases phosphorylate a human cell DNA replication factor, RPA, and activate DNA replication. *EMBO J*, 11, 2189-2199.
29. Oakley, G.G., Patrick, S.M., Yao, J., Carty, M.P., Turchi, J.J. and Dixon, K. (2003) RPA phosphorylation in mitosis alters DNA binding and protein-protein interactions. *Biochemistry*, 42, 3255-3264.
30. Fang, F. and Newport, J.W. (1993) Distinct roles of cdk2 and cdc2 in RP-A phosphorylation during the cell cycle. *J Cell Sci*, 106 (Pt 3), 983-994.
31. Lee, S.H. and Kim, D.K. (1995) The role of the 34-kDa subunit of human replication protein A in simian virus 40 DNA replication in vitro. *J Biol Chem*, 270, 12801-12807.
32. Henricksen, L.A. and Wold, M.S. (1994) Replication protein A mutants lacking phosphorylation sites for p34cdc2 kinase support DNA replication. *J Biol Chem*, 269, 24203-24208.

33. Binz, S.K. and Wold, M.S. (2008) Regulatory Functions of the N-terminal Domain of the 70-kDa Subunit of Replication Protein A (RPA). *J Biol Chem*, 283, 21559-21570.
34. Alderton, G.K., Joenje, H., Varon, R., Borglum, A.D., Jeggo, P.A. and O'Driscoll, M. (2004) Seckel syndrome exhibits cellular features demonstrating defects in the ATR-signalling pathway. *Hum Mol Genet*, 13, 3127-3138.
35. Kozlov, S.V., Graham, M.E., Peng, C., Chen, P., Robinson, P.J. and Lavin, M.F. (2006) Involvement of novel autophosphorylation sites in ATM activation. *EMBO J*, 25, 3504-3514.
36. Stiff, T., Walker, S.A., Cerosaletti, K., Goodarzi, A.A., Petermann, E., Concannon, P., O'Driscoll, M. and Jeggo, P.A. (2006) ATR-dependent phosphorylation and activation of ATM in response to UV treatment or replication fork stalling. *EMBO J*, 25, 5775-5782.
37. Zhang, N., Chen, P., Khanna, K.K., Scott, S., Gatei, M., Kozlov, S., Watters, D., Spring, K., Yen, T. and Lavin, M.F. (1997) Isolation of full-length ATM cDNA and correction of the ataxia-telangiectasia cellular phenotype. *Proc Natl Acad Sci USA*, 94, 8021-8026.
38. Nasheuer, H.P., Moore, A., Wahl, A.F. and Wang, T.S. (1991) Cell cycle-dependent phosphorylation of human DNA polymerase alpha. *J Biol Chem*, 266, 7893-7903.
39. Bauerschmidt, C., Pollok, S., Kremmer, E., Nasheuer, H.P. and Grosse, F. (2007) Interactions of human Cdc45 with the Mcm2-7 complex, the GINS complex, and DNA polymerases delta and epsilon during S phase. *Genes Cells*, 12, 745-758.
40. Cruet-Hennequart, S., Coyne, S., Glynn, M.T., Oakley, G.G. and Carty, M.P. (2006) UV-induced RPA phosphorylation is increased in the absence of DNA polymerase eta and requires DNA-PK. *DNA Repair (Amst)*, 5, 491-504.
41. Leahy, J.J., Golding, B.T., Griffin, R.J., Hardcastle, I.R., Richardson, C., Rigoreau, L. and Smith, G.C. (2004) Identification of a highly potent and selective DNA-dependent protein kinase (DNA-PK) inhibitor (NU7441) by screening of chromenone libraries. *Bioorg Med Chem Lett*, 14, 6083-6087.
42. Veuger, S.J., Curtin, N.J., Richardson, C.J., Smith, G.C. and Durkacz, B.W. (2003) Radiosensitization and DNA repair inhibition by the combined use of novel inhibitors of DNA-dependent protein kinase and poly(ADP-ribose) polymerase-1. *Cancer Res*, 63, 6008-6015.
43. Hickson, I., Zhao, Y., Richardson, C.J., Green, S.J., Martin, N.M.B., Orr, A.I., Reaper, P.M., Jackson, S.P., Curtin, N.J. and Smith, G.C.M. (2004) Identification and characterization of a novel and specific inhibitor of the ataxia-telangiectasia mutated kinase ATM. *Cancer Res*, 64, 9152.
44. Meijer, L. and Raymond, E. (2003) Roscovitine and other purines as kinase inhibitors. From starfish oocytes to clinical trials. *Acc Chem Res*, 36, 417-425.
45. Henricksen, L.A., Umbricht, C.B. and Wold, M.S. (1994) Recombinant replication protein A: expression, complex formation, and functional characterization. *J Biol Chem*, 269, 11121-11132.
46. Nasheuer, H.P., von Winkler, D., Schneider, C., Dornreiter, I., Gilbert, I. and Fanning, E. (1992) Purification and functional characterization of bovine RP-A in an in vitro SV40 DNA replication system. *Chromosoma*, 102, S52-59.
47. Voitenleitner, C., Fanning, E. and Nasheuer, H.P. (1997) Phosphorylation of DNA polymerase alpha-primase by cyclin A-dependent kinases regulates initiation of DNA replication in vitro. *Oncogene*, 14, 1611-1615.

48. Dehde, S., Rohaly, G., Schub, O., Nasheuer, H.P., Bohn, W., Chemnitz, J., Deppert, W. and Dornreiter, I. (2001) Two immunologically distinct human DNA polymerase alpha-primase subpopulations are involved in cellular DNA replication. *Mol Cell Biol*, 21, 2581-2593.
49. Schub, O., Rohaly, G., Smith, R.W., Schneider, A., Dehde, S., Dornreiter, I. and Nasheuer, H.P. (2001) Multiple phosphorylation sites of DNA polymerase alpha-primase cooperate to regulate the initiation of DNA replication in vitro. *J Biol Chem*, 276, 38076-38083.
50. Pestryakov, P.E., Weisshart, K., Schlott, B., Khodyreva, S.N., Kremmer, E., Grosse, F., Lavrik, O.I. and Nasheuer, H.P. (2003) Human replication protein A. The C-terminal RPA70 and the central RPA32 domains are involved in the interactions with the 3'-end of a primer-template DNA. *J Biol Chem*, 278, 17515-17524.
51. Weisshart, K., Pestryakov, P., Smith, R.W., Hartmann, H., Kremmer, E., Lavrik, O. and Nasheuer, H.P. (2004) Coordinated regulation of replication protein A activities by its subunits p14 and p32. *J Biol Chem*, 279, 35368-35376.
52. Harlow, E. and Lane, D. (1988) *Antibodies: A Laboratory Manual*. Cold Spring Harbor Laboratory Cold Spring Harbor, NY.
53. Weisshart, K., Forster, H., Kremmer, E., Schlott, B., Grosse, F. and Nasheuer, H.P. (2000) Protein-protein interactions of the primase subunits p58 and p48 with simian virus 40 T antigen are required for efficient primer synthesis in a cell-free system. *J Biol Chem*, 275, 17328-17337.
54. Elowe, S., Hummer, S., Uldschmid, A., Li, X. and Nigg, E.A. (2007) Tension-sensitive Plk1 phosphorylation on BubR1 regulates the stability of kinetochore microtubule interactions. *Genes Dev*, 21, 2205-2219.
55. Kwon, Y.G., Lee, S.Y., Choi, Y., Greengard, P. and Nairn, A.C. (1997) Cell cycle-dependent phosphorylation of mammalian protein phosphatase 1 by cdc2 kinase. *Proc Natl Acad Sci USA*, 94, 2168-2173.
56. Brush, G.S., Clifford, D.M., Marinco, S.M. and Bartrand, A.J. (2001) Replication protein A is sequentially phosphorylated during meiosis. *Nucleic Acids Res*, 29, 4808-4817.
57. Murti, K.G., He, D.C., Brinkley, B.R., Scott, R. and Lee, S.H. (1996) Dynamics of human replication protein A subunit distribution and partitioning in the cell cycle. *Exp Cell Res*, 223, 279-289.
58. Loo, Y.M. and Melendy, T. (2000) The majority of human replication protein A remains complexed throughout the cell cycle. *Nucleic Acids Res*, 28, 3354-3360.
59. Stephan, H. (2007) Human replication protein A in the cell cycle and DNA damage response, NUI Galway, Galway, Ireland.
60. Kim, E.H., Kim, S.U., Shin, D.Y. and Choi, K.S. (2004) Roscovitine sensitizes glioma cells to TRAIL-mediated apoptosis by downregulation of survivin and XIAP. *Oncogene*, 23, 446-456.
61. Mgbonyebi, O.P., Russo, J. and Russo, I.H. (1999) Roscovitine induces cell death and morphological changes indicative of apoptosis in MDA-MB-231 breast cancer cells. *Cancer Res*, 59, 1903-1910.
62. Kaufmann, W.K. (2007) Initiating the uninitiated: replication of damaged DNA and carcinogenesis. *Cell Cycle*, 6, 1460-1467.
63. Cheng, X., Cheong, N., Wang, Y. and Iliakis, G. (1996) Ionizing radiation-induced phosphorylation of RPA p34 is deficient in ataxia telangiectasia and reduced in aged normal fibroblasts. *Radiother Oncol*, 39, 43-52.
64. Oakley, G.G., Loberg, L.I., Yao, J., Risinger, M.A., Yunker, R.L., Zernik-Kobak, M., Khanna, K.K., Lavin, M.F., Carty, M.P. and Dixon, K. (2001) UV-

induced hyperphosphorylation of replication protein a depends on DNA replication and expression of ATM protein. *Mol Biol Cell*, 12, 1199-1213.

65. Sarkaria, J.N., Tibbetts, R.S., Busby, E.C., Kennedy, A.P., Hill, D.E. and Abraham, R.T. (1998) Inhibition of phosphoinositide 3-kinase related kinases by the radiosensitizing agent wortmannin. *Cancer Res*, 58, 4375-4382.
66. Wang, H., Guan, J., Wang, H., Perrault, A.R., Wang, Y. and Iliakis, G. (2001) Replication protein A2 phosphorylation after DNA damage by the coordinated action of ataxia telangiectasia-mutated and DNA-dependent protein kinase. *Cancer Res*, 61, 8554-8563.
67. Anantha, R.W., Sokolova, E. and Borowiec, J.A. (2008) RPA phosphorylation facilitates mitotic exit in response to mitotic DNA damage. *Proc Natl Acad Sci USA*, 105, 12903-12908.
68. Huang, X., Tran, T., Zhang, L., Hatcher, R. and Zhang, P. (2005) DNA damage-induced mitotic catastrophe is mediated by the Chk1-dependent mitotic exit DNA damage checkpoint. *Proc Natl Acad Sci USA*, 102, 1065-1070.
69. Mikhailov, A., Cole, R.W. and Rieder, C.L. (2002) DNA damage during mitosis in human cells delays the metaphase/anaphase transition via the spindle-assembly checkpoint. *Curr Biol*, 12, 1797-1806.
70. Smits, V.A., Klompmaker, R., Arnaud, L., Rijksen, G., Nigg, E.A. and Medema, R.H. (2000) Polo-like kinase-1 is a target of the DNA damage checkpoint. *Nat Cell Biol*, 2, 672-676.
71. Jazayeri, A., Falck, J., Lukas, C., Bartek, J., Smith, G.C., Lukas, J. and Jackson, S.P. (2006) ATM- and cell cycle-dependent regulation of ATR in response to DNA double-strand breaks. *Nat Cell Biol*, 8, 37-45.
72. Rainey, M.D., Black, E.J., Zachos, G. and Gillespie, D.A. (2007) Chk2 is required for optimal mitotic delay in response to irradiation-induced DNA damage incurred in G(2) phase. *Oncogene*.
73. Syljuasen, R.G., Jensen, S., Bartek, J. and Lukas, J. (2006) Adaptation to the ionizing radiation-induced G2 checkpoint occurs in human cells and depends on checkpoint kinase 1 and Polo-like kinase 1 kinases. *Cancer Res*, 66, 10253-10257.
74. Zachos, G., Black, E.J., Walker, M., Scott, M.T., Vagnarelli, P., Earnshaw, W.C. and Gillespie, D.A. (2007) Chk1 is required for spindle checkpoint function. *Dev Cell*, 12, 247-260.

SUPPLEMENTARY MATERIAL

MATERIALS AND METHODS

Purification of RPA2 CDK phosphorylation mutants - Human recombinant RPA2wt (wild type) and its alanine mutants RPA2- S23A, RPA2- S29A and RPA2-S23A/S29A were expressed as RPA heterotrimer and purified as described previously (Henricksen et al., 1994). Expression vectors for all mutant RPA2 proteins were kindly provided by Dr. Klaus Weisshart.

Subcellular fractionation using DNase I treatment – Cells were fractionated as described in Material and Methods" in "soluble fraction" and "wash fraction". The pellet was then resuspended in 1 ml DNase I digest buffer (20 mM Hepes [pH 7.5], 150 mM NaCl, 2 mM $MgCl_2$, supplemented with DNase I (1 µg), 10 mM NaF, 1 mM Na_3VO_4, 10 mM β-glycerophosphate, 1× Phosphatase Inhibitor Cocktail I and 1× Protease Inhibitor Cocktail) and incubated for 3 h at 4ºC with agitation. Samples were subsequently centrifuged at 14,000×*g* for 10 min at 4°C and the supernatant referred to as "chromosomal-bound fraction". The pellet was washed in digest buffer once and after centrifugation this supernatant was discarded. The remaining pellet was resupended in 1 ml homogenization buffer (20 mM Hepes [pH 7.5], 1% SDS 150 mM NaCl, 1 mM $MgCl_2$, 0.5 mM EDTA supplemented with 1 mM DTT, 10 mM NaF, 1 mM Na_3VO_4, 10 mM β-glycerophosphate, 1× Phosphatase Inhibitor Cocktail I and 1× Protease Inhibitor Cocktail) and referred to as "insoluble fraction".

Cell viability assay – For cell viability analysis, cells were stained with propidium iodide (PI) (1 µg/ml) and incubated for 5 minutes on ice followed by flow cytometry analysis (FACScan; Becton Dickinson, USA). To determine cell viability the number of PI-positive cells and total cell numbers were measured. In addition, cells were stained with trypan blue. Total cell numbers and stained cells were counted using a conventional light microscope. The data are presented as the ratio between stained cells to total cell numbers and as the mean+/-S.E.M. of at least three independent experiments.

Figure S1. Characterization of phosphospecific RPA2 antibodies using a Cdk1-cyclin B *in vitro* kinase assay. Immuno dot-blot showing the specificity of anti-RPA2-(P)-S23 and anti-RPA2-(P)-S29 antibodies. *In vitro* phosphorylation reactions were carried using 100 ng of purified recombinant RPA2 wild type (wt) or RPA2 alanine mutants (RPA2-S23A, RPA2- S29A and RPA2-S23A/S29A) as indicated in the presence or absence of 2 µg of purified Cdk1-cyclin B. The kinase reactions were immediately transferred on a nitrocellulose membrane using a dot-blotter (BioRad). The membranes were probed with phosphospecific anti-RPA2-(P)-S29, anti-RPA2-(P)-S23 and total RPA2 antibodies. Anti-cyclin B detection served as a control. The immunodection was merged with a grid explaining the respective RPA proteins, which are present.

Figure S2. Immunolocalization of total and mitotically phosphorylated RPA2 at different stages of M-phase. RPA2 was detected using anti-RPA2-(P)-S23, anti-RPA2-(P)-S29 (both phosphospecific antibodies), and total anti-RPA2 [RBF-4E4] primary antibodies and Cy3-labelled secondary antibodies. Spindle microtubules were detected using anti-α-tubulin primary antibodies and Cy2-labelled secondary antibodies. DNA was counterstained with ToPro3. All images were analyzed by confocal microscopy and present as a single representative stack.

Figure S3. Analysis of RPA during mitosis. A. Immunolocalization of RPA1 and RPA3 subunits in mitosis. Images show the localization of total RPA1 and RPA3 in metaphase using anti-RPA1 and anti-RPA3 antibodies, respectively, and Cy3-labelled secondary antibodies. Cells from an asynchronous population were fixed, stained with the respective antibodies, and DNA was counterstained with ToPro3. Spindle microtubules were detected using anti-α-tubulin primary antibodies and Cy2-labelled secondary antibodies. All images were analyzed by confocal microscopy and present as a single representative stack. **B.** Subcellular fractionation of mock- or IR-treated mitotic cells using DNAse I. Subcellular localization of mitotic cells mock-treated or exposed to IR (10 Gy). RPA was detected using RPA antibodies as indicated. H3-(P)-S10, GAPDH and Vimentin antibodies were used as controls. Abbreviations used in the figure: T = whole cell lysates, SF = soluble fraction, WF = wash fraction, CF = chromosomal bound fraction and IF = insoluble fraction.

Figure S4. Viability of mock- or IR-treated HeLa S3 cells. Mitotic arrested HeLa S3 cells were mock- or IR-treated (10 Gy) and subsequently released from the arrest and harvested at indicated time points under identical conditions as described in Fig. 4A. The cell viability was determined as the number of detected PI-positive cells using a flow cytometer (*left panel*) or trypan blue positive cells, which were counted under a conventional light microscope (*right panel*). The data are presented as the ratio of stained cells to total cell number with mean+/-S.E.M. of at least three independent experiments.

Figure S5. Quantification of mitotic RPA2 phosphorylation. The quantification of mitotically phosphorylated RPA2 (band labeled with *mp*) of Fig. 4A was performed using Scion Image software (Scion Corporation, Maryland, USA) and presented as relative intensity (%). The intensity of band marked as *mp* of 0h in mock-treated cells in Fig. 4A was arbitrarily set as 100%.

Figure S6. Viability of mock- or IR-treated HeLa S3 cells in the absence or presence of PI3K-like kinase inhibitors. HeLa S3 cells were pre-incubated in the absence or presence of wortmannin (10μM), ATM inhibitor KU-55933 (10μM), DNA-PK inhibitor NU7441 (10μM) and DMSO as the solvent control 1 h prior to mock or IR treatment (10 Gy), followed by continuation of drug treatment. Cells were harvested at indicated time points and cell viability was determined as the number of detected PI-positive cells using a flow cytometer. The data are presented as the ratio of stained cells to total cell number with mean+/-S.E.M. of at least three independent experiments.

REFERENCES

1. Henricksen, L.A., Umbricht, C.B. and Wold, M.S. (1994) Recombinant replication protein A: expression, complex formation, and functional characterization. *J. Biol. Chem.*, **269**, 11121-11132.

Fig. 1

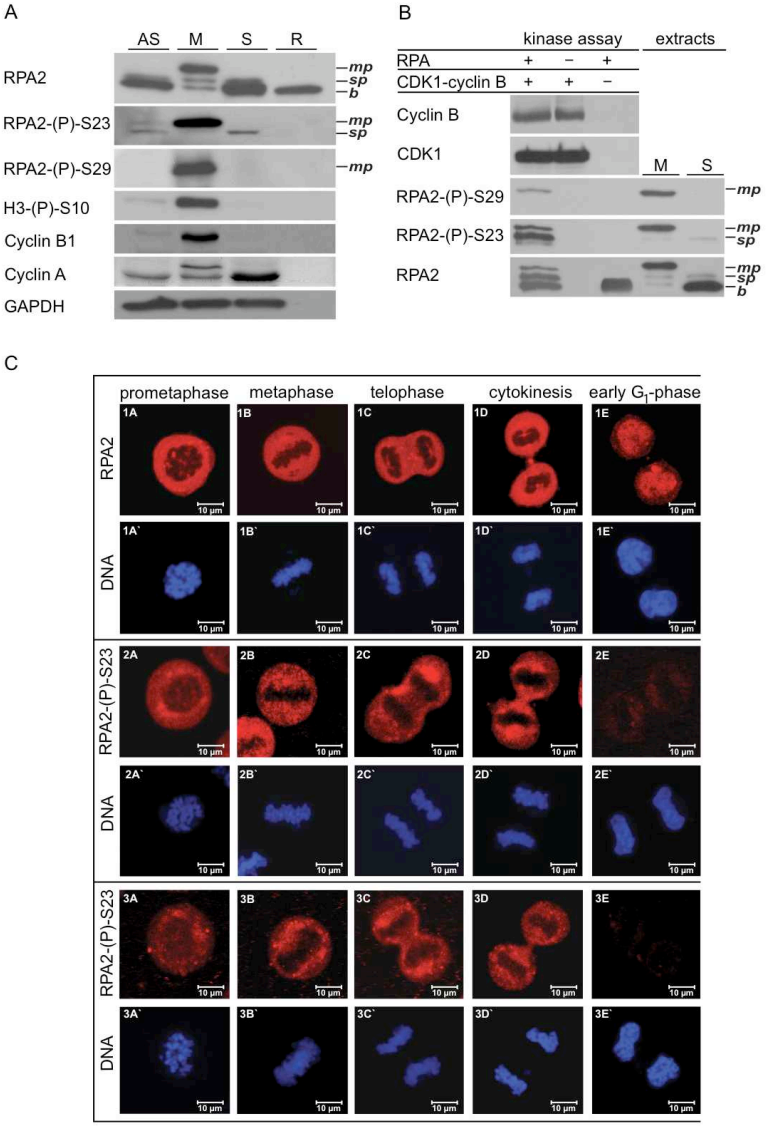

100x142mm (300 x 300 DPI)

Fig. 2

A

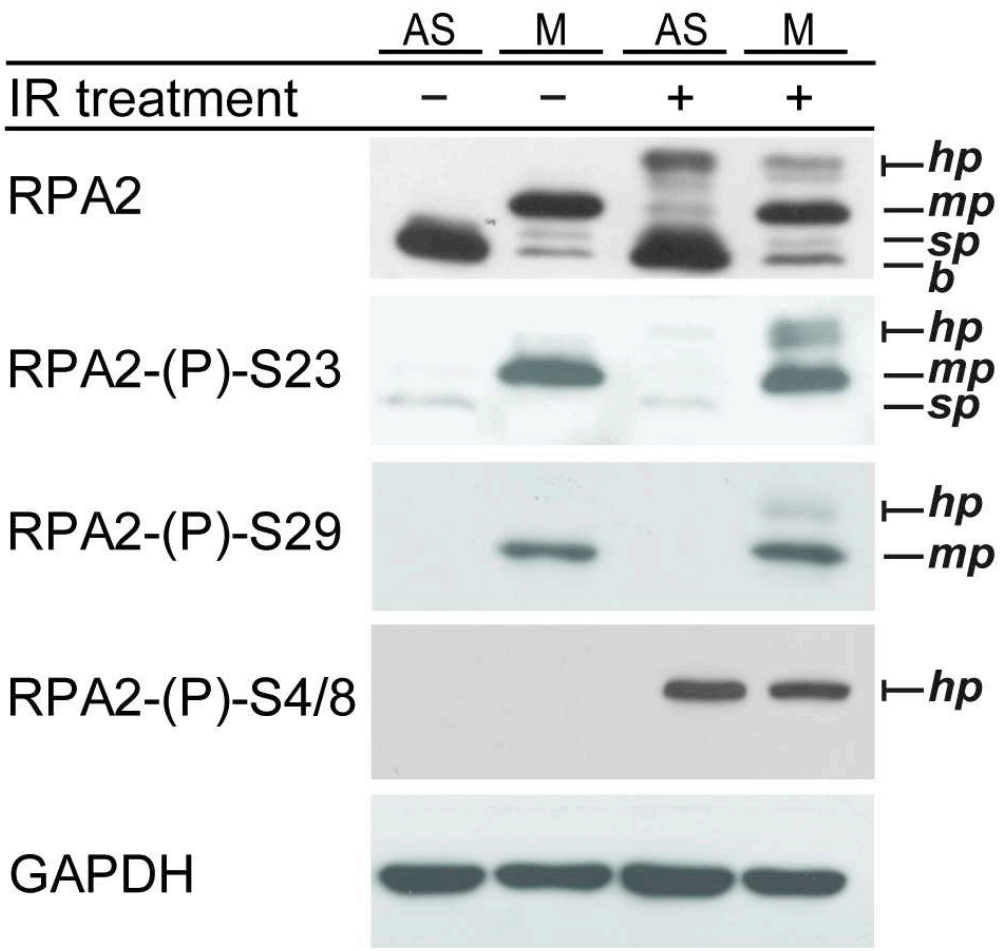

80x91mm (300 x 300 DPI)

Fig. 3

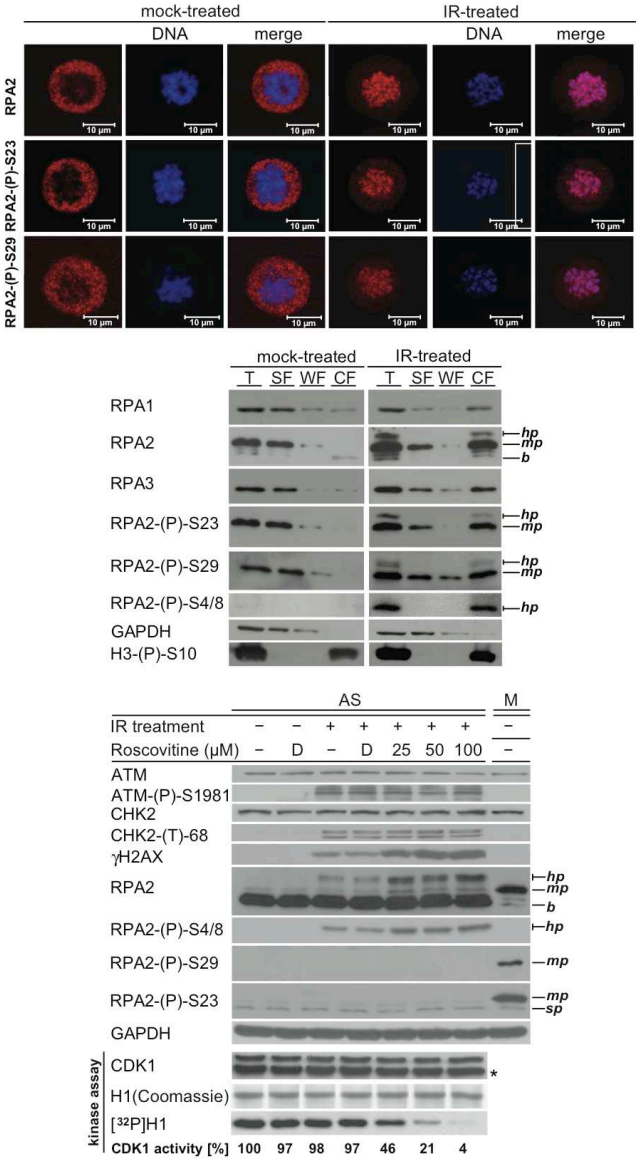

100x142mm (300 x 300 DPI)

Fig. 4

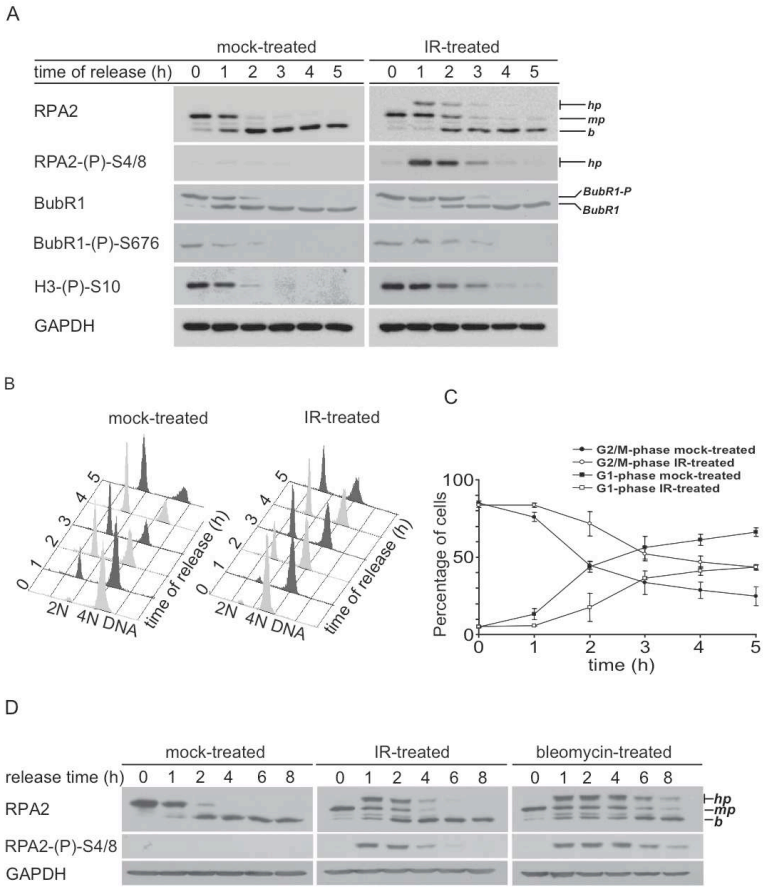

100x142mm (300 x 300 DPI)

Fig. 5

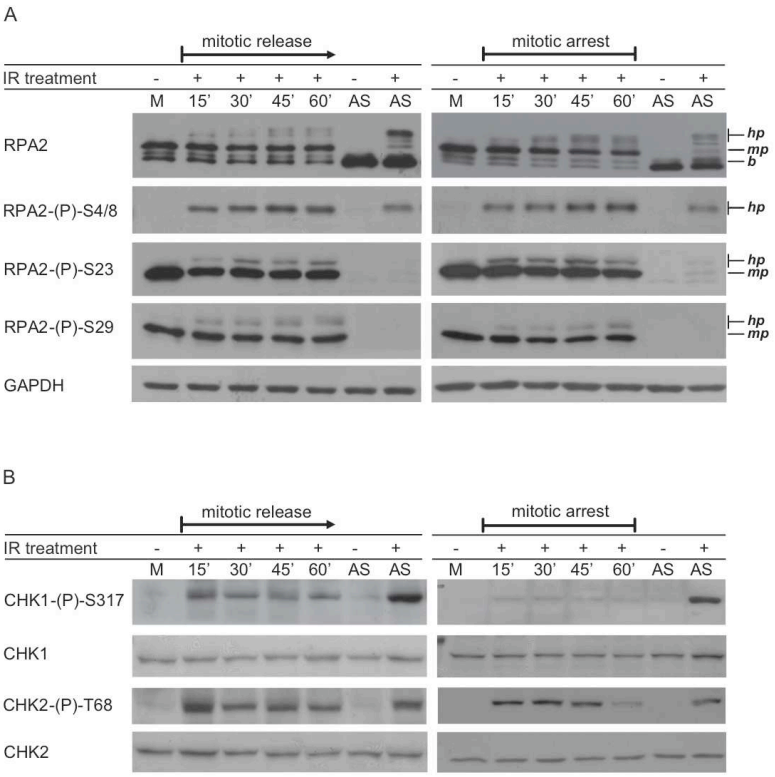

100x142mm (300 x 300 DPI)

Fig. 6

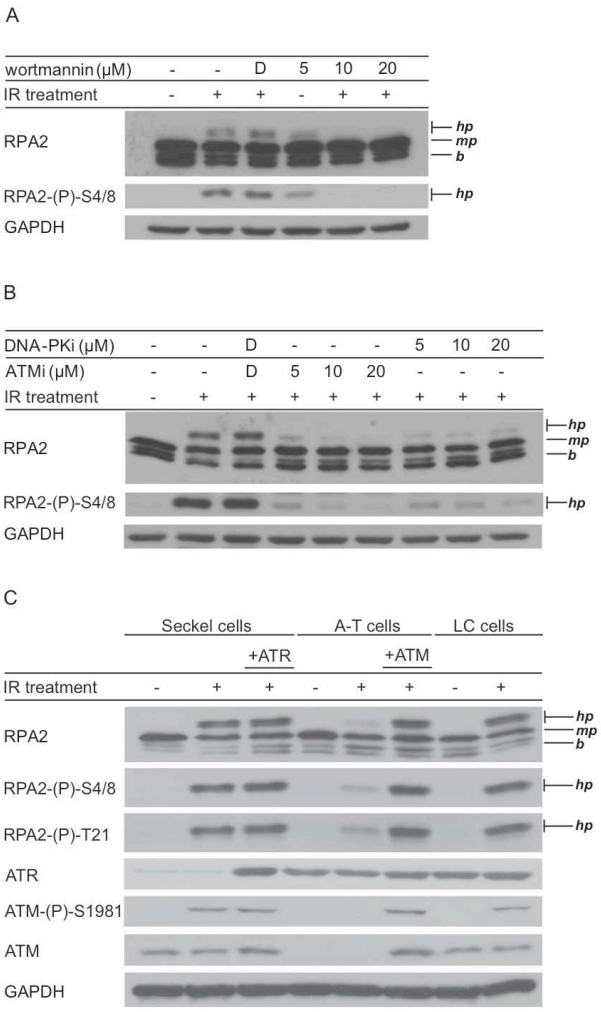

100x142mm (300 x 300 DPI)